J. Fluid Mech. (1990), *vol.* 210, *pp.* 183–199
Printed in Great Britain

Numerical simulation of interactions between Görtler vortices and Tollmien–Schlichting waves

By M. R. MALIK[1] AND M. Y. HUSSAINI[2]

[1] High Technology Corporation, P.O. Box 7262, Hampton, Virginia 23666, USA
[2] ICASE, NASA Langley Research Center, Hampton, Virginia 23665, USA

(Received 17 January 1989)

The problem of nonlinear development of Görtler vortices and interaction with Tollmien–Schlichting waves is considered within the framework of incompressible Navier–Stokes equations which are solved by a Fourier–Chebyshev spectral method. It is shown that two-dimensional waves can be excited in the flow modulated by Görtler vortices. Owing to nonlinear effects, this interaction further leads to the development of oblique waves with spanwise wavelength equal to the Görtler vortex wavelength. Interaction is also considered of oblique waves with spanwise wavelength twice that of Görtler vortices.

1. Introduction

The subject of laminar/turbulent transition is of fundamental and practical importance in fluid mechanics. An in-depth knowledge of the transition mechanism is needed not only for boundary/shear layer control (e.g. delay of transition or mixing enhancement), but also for understanding of turbulence. Depending on the state of the boundary layer, various instability mechanisms such as Tollmien–Schlichting (TS), crossflow and Görtler vortices may be operative. Which instability modes are actually excited in a boundary layer depends a great deal upon the particular 'forcing' present. This is the classical 'receptivity' problem. The presence of a finite-amplitude disturbance in a boundary layer would also lead to the excitation of disturbance modes which may otherwise be damped or weakly unstable according to linear stability theory. Examples of such interactions are the possible excitation of TS instability in the presence of Görtler vortices on a concave wall, fundamental or subharmonic secondary instability in a flat-plate boundary layer or the excitation of TS instability in the presence of crossflow vortices on a swept wing.

Consider a boundary-layer flow on a concavely curved plate. Here, counter-rotating steady Görtler vortices form owing to centrifugal instability. If the Reynolds number is high enough, TS instability may also be present. Nonlinear development of Görtler vortices and Görtler/TS interaction is a problem of both fundamental and practical importance. The interaction may take place in three different situations: (i) when Görtler vortices are of finite amplitude and TS waves are infinitesimally small; (ii) when TS waves are of finite amplitude and Görtler vortices are weak; (iii) when both Görtler vortices and TS waves are of finite amplitude so that they interact nonlinearly.

Nayfeh (1981), using multiple-scale analysis for two-dimensional boundary layers, showed that a finite-amplitude Görtler vortex could interact with two oblique TS waves of spanwise wavelength twice that of the Görtler vortex. The resulting growth

rates were found to be many times larger than the linear theory growth rate of the TS wave without the Görtler vortex. Furthermore, these exponential growth rates were predicted to increase with increasing amplitude of the vortex. Since the amplitude of the vortex increases exponentially, there is essentially a 'double exponential growth' of the disturbances in the boundary layer. Similar results were also obtained by Srivastava & Dallmann (1987). The concept of 'double exponential growth' has also been suggested by Herbert & Morkovin (1979) for the interaction of finite-amplitude TS waves with streamwise vortices and by Floryan & Saric (1980) for the streamwise vortices interacting with Görtler vortices. Recently Hall & Smith (1988) have also studied Görtler/TS interaction. Such interactions are crucially dependent on the amplitude of the primary mode. The present study is an attempt to determine the amplitudes of the primary instability for these interactions to take place. Other types of interactions including those which involve oblique TS waves with spanwise wavelength equal to the Görtler vortex wavelength are also discussed.

In this work, the wave-interaction problem in two-dimensional boundary layers on a concave surface is studied numerically. The three-dimensional incompressible Navier–Stokes equations are solved by a Fourier–Chebyshev spectral method with two periodic and one non-periodic direction. Even though the boundary layer grows spatially, the works of Wray & Hussaini (1984), Zang & Hussaini (1985) and Spalart (1984) have shown that temporal solution of the Navier–Stokes equations with periodic boundary conditions in the streamwise direction is able to capture the qualitative features of the transition process on a flat plate quite adequately. It is assumed that such will be the case in the boundary layer that is considered here. Though the method is applicable to all the regimes of interaction listed above, results are presented only for the case where Görtler vortices are finite-amplitude but TS waves have relatively small amplitude.

2. Governing equations and numerical approach

We consider the problem of laminar/turbulent transition in two- and three-dimensional boundary layers. The governing Navier–Stokes equations for an incompressible fluid are

$$\boldsymbol{U}_t + \boldsymbol{U}\cdot\nabla\boldsymbol{U} = -\nabla p + \nu\nabla^2\boldsymbol{U} + \boldsymbol{F}, \tag{2.1}$$

$$\nabla\cdot\boldsymbol{U} = 0, \tag{2.2}$$

where $\boldsymbol{U} = (u, v, w)$ is the velocity vector, p the pressure, and ν the kinematic viscosity. The term $\boldsymbol{F}$ is a forcing term. No-slip boundary conditions at the solid wall ($z = 0$) are imposed, i.e.

$$\boldsymbol{U}(x, y, 0, t) = 0. \tag{2.3}$$

In the free stream, it is reasonable to require that

$$\boldsymbol{U} \to \boldsymbol{U}_\infty \quad \text{as} \quad z \to \infty. \tag{2.4}$$

Equations (2.1)–(2.4) are solved by a Fourier–Chebyshev spectral method similar to that described by Malik, Zang & Hussaini (1985). Periodicity is assumed in the x- and y-directions. The dependent variables have Fourier–Chebyshev series of the form

$$u(x, y, z, t) = \sum_{k_x=-\frac{1}{2}K_x}^{\frac{1}{2}K_x-1} \sum_{k_y=-\frac{1}{2}K_y}^{\frac{1}{2}K_y-1} \sum_{n=0}^{N} \hat{u}(t)\, \mathrm{e}^{2\pi\mathrm{i}(k_x x/L_x)}\, \mathrm{e}^{2\pi\mathrm{i}(k_y y/L_y)} T_n(\eta), \tag{2.5}$$

where L_x and L_y are the periodicity lengths in the x- and y-directions, respectively, and T_n is the Chebyshev polynomial of degree n. The normal computational coordinate η is related to z through the algebraic transformation

$$z = a\frac{1+\eta}{1+\dfrac{2a}{z_\infty}-\eta}, \tag{2.6}$$

where a is a scaling constant used for proper distribution of points within the boundary layer and z_∞ is the location where free-stream asymptotic boundary conditions (Malik *et al.* 1985) are imposed.

The spatial discretization employs spectral collocation. The collocation points for the periodic directions are

$$x_j = jL_x/K_x, \qquad j = 0, 1, \ldots, K_x - 1, \tag{2.7}$$

$$y_m = mL_y/K_y, \quad m = 0, 1, \ldots, K_y - 1. \tag{2.8}$$

A staggered grid is employed in the normal direction. Velocities are defined at the points

$$\eta_q = \cos\left(\frac{\pi q}{N}\right), \quad q = 0, 1, \ldots, N, \tag{2.9}$$

and the pressures at

$$\eta_{q+\frac{1}{2}} = \cos\left(\frac{\pi(q+\frac{1}{2})}{N}\right), \quad q = 0, 1, \ldots, N-1. \tag{2.10}$$

No artificial pressure boundary conditions are therefore needed. The momentum equations are imposed at the points given by (2.9) and the continuity at those given by (2.10).

In the spectral collocatioin method, spatial derivatives of u are obtained by differentiating the series expansion coefficients $\hat{u}(t)$ determined by discrete Fourier and Chebyshev transform of the grid-point values of u. The temporal discretization involves Crank–Nicolson on the pressure gradient and vertical diffusion terms. The remaining terms in the momentum equations are handled explicitly by the second-order-accurate Adams–Bashforth method. The incompressibility constraint is imposed implicitly. The resulting implicit equations are solved iteratively by a minimum residual method. The details of the procedure can be found in Malik *et al.* (1985) and Canuto *et al.* (1988).

2.1. *Flow over a curved wall*

The numerical procedure outlined above is applicable to the study of a transition problem in two- and three-dimensional boundary layers where TS, Görtler or crossflow instability mechanisms may be operative. Here we describe the application of the method to the flow over a concavely curved plate where both Görtler vortices and TS waves might exist. Extension to three-dimensional boundary layers is straightforward.

Consider an incompressible flow with free-stream velocity U_∞ along a mildly curved wall with constant curvature $\kappa = l/r$ where l is a characteristic lengthscale and r is the radius of curvature of the wall. If x is the distance along the curved wall,

y along the span, and z normal to the wall, then the governing equations (2.1) and (2.2) may be represented in body-oriented coordinates as

$$\frac{\partial u}{\partial t}+\lambda u\frac{\partial u}{\partial x}+v\frac{\partial u}{\partial y}+w\frac{\partial u}{\partial z}+\gamma uw=-\lambda\frac{\partial p}{\partial x}+\nu\left[\nabla^2 u+\gamma\frac{\partial u}{\partial z}-\gamma^2 u+2\gamma\lambda\frac{\partial w}{\partial x}\right], \quad (2.11)$$

$$\frac{\partial v}{\partial t}+\lambda u\frac{\partial v}{\partial x}+v\frac{\partial v}{\partial y}+w\frac{\partial v}{\partial z}=-\frac{\partial p}{\partial y}+\nu\left[\nabla^2 v+\gamma\frac{\partial v}{\partial z}\right], \quad (2.12)$$

$$\frac{\partial w}{\partial t}+\lambda u\frac{\partial w}{\partial x}+v\frac{\partial w}{\partial y}+w\frac{\partial w}{\partial z}-\gamma u^2=-\frac{\partial p}{\partial z}+\nu\left[\nabla^2 w+\gamma\frac{\partial w}{\partial z}-\gamma^2 w-2\gamma\lambda\frac{\partial u}{\partial x}\right], \quad (2.13)$$

$$\lambda\frac{\partial u}{\partial x}+\frac{\partial v}{\partial y}+\frac{\partial w}{\partial z}+\gamma w=0, \quad (2.14)$$

where $$\nabla^2=\lambda^2\frac{\partial^2}{\partial x^2}+\frac{\partial^2}{\partial y^2}+\frac{\partial^2}{\partial z^2}, \quad \lambda=\frac{1}{1+\kappa z}, \quad \gamma=\frac{k}{1+\kappa z}.$$

In (2.11)–(2.14), all velocities are scaled by U_∞, lengths by l, time by l/U_∞, pressure by ρU_∞^2; $\nu=1/R$, where R is the Reynolds number. A Görtler number can be defined as $G=R|\kappa|^{\frac{1}{2}}$.

According to first-order boundary-layer theory, the above equations reduce to the Blasius flow which provides the basic flow for our study of Görtler/TS interaction and transition simulation in a two-dimensional boundary layer.

2.2. *Linear stability theory*

We consider an infinitesimally small disturbance superimposed on the Blasius flow. For instance, the streamwise velocity $u(x,y,z,t)$ may be written as

$$u(x,y,z,t)=U_{\mathrm{B}}(z)+\epsilon\hat{u}(z)\,\mathrm{e}^{\mathrm{i}(\alpha x+\beta y-\omega t)} \quad (2.15)$$

under the quasi-parallel flow assumption. Here ϵ is a small parameter, α and β are the disturbance wavenumbers in the x- and y-directions respectively and $\omega=\omega_{\mathrm{r}}+\mathrm{i}\omega_{\mathrm{i}}$ is complex frequency. The real part ω_{r} is the actual disturbance frequency and the imaginary part ω_{i} is the temporal growth rate. If $\omega_{\mathrm{i}}>0$ the disturbance amplitude increases; otherwise, the disturbance decays.

Linear stability equations may be derived by substituting $u(x,y,z,t)$ from (2.15) and similar expressions for other dependent variables into the Navier–Stokes equations (2.11)–(2.14) and then retaining only terms of $O(\epsilon)$. The resulting sixth-order system of ordinary differential equations describes an eigenvalue problem for parameters α, β and ω which is solved by a fourth-order-accurate compact difference scheme of Malik, Chuang & Hussaini (1982). Depending upon the values of the Görtler number G and wavenumbers α, β, the governing equations yield a solution for both Görtler vortices and TS waves. These solutions provide the initial conditions for the nonlinear calculations. In figures 1 and 2, described below, we provide linear results for Görtler and TS waves to emphasize the differences between the two instabilities.

2.3. *Nonlinear simulations*

Various nonlinear problems may now be formulated. Suppose, we are interested in studying the nonlinear development of Görtler vortices. We solve the linear stability

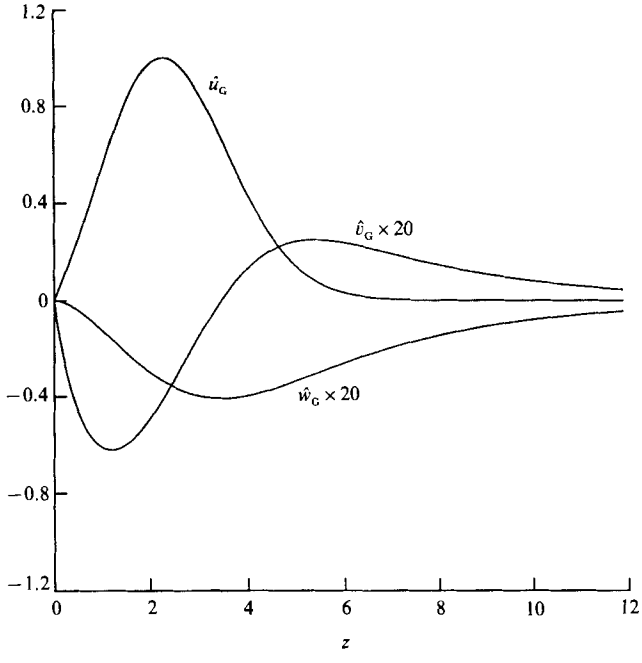

FIGURE 1. Eigenfunctions for a Görtler vortex in a Blasius boundary layer: $G = 14$, $\beta = 0.3$.

problem for the Blasius boundary layer and find $\beta = \beta_G$, the growth rate ω_i and the disturbance eigenfunctions $\hat{u}_G, \hat{v}_G, \hat{w}_G$. These are presented in figure 1. The plots show that the streamwise component $\hat{u}_G$ is an order-of-magnitude larger than the cross-stream components $\hat{v}_G$ and $\hat{w}_G$. The spanwise component is 90° out of phase with $\hat{u}_G$ and $\hat{v}_G$. This allows the steady Görtler vortex problem to be represented as a system of real equations. In the present case, our complex system of equations automatically yields the real solution for the steady Görtler vortex. The structure of $\hat{v}_G$ and $\hat{w}_G$ is such that it results in a pair of counter-rotating vortices. There are higher eigenstates for the Görtler problem which yield multiple sets of counter-rotating vortices stacked on top of each other. How these higher modes would interact with TS mode may be of interest. The linear stability theory also yields unsteady Görtler vortices, whose interaction with TS waves may be of significance, particularly in the later stages of transition. Here, however, we only consider the steady Görtler vortices. Görtler vortices found in experiments are usually steady and of first-mode type. In the present study, the steady Görtler vortex is assigned an initial finite amplitude ϵ_G. Then an initial condition, say for the x-component of velocity, is of the form

$$u(x, y, z, 0) = U_B(z) + \epsilon_G \,\mathrm{Re}\,[\hat{u}_G(z)\, e^{i\beta_G y}]. \tag{2.16}$$

Equations (2.11)–(2.14) are solved with these initial conditions and the solution is marched in time. The solution yields the development of the fundamental and various harmonics depending upon the number of modes allowed in the simulation according to (2.5). In the linear regime, the temporal development is related to the spatial development through group velocity transformation ($C_g = \partial\omega/\partial\alpha$) as for TS waves.

The eigenfunctions for a TS wave are presented in figure 2. The eigenfunctions are now complex with disturbance peak lying closer to the solid boundary. The

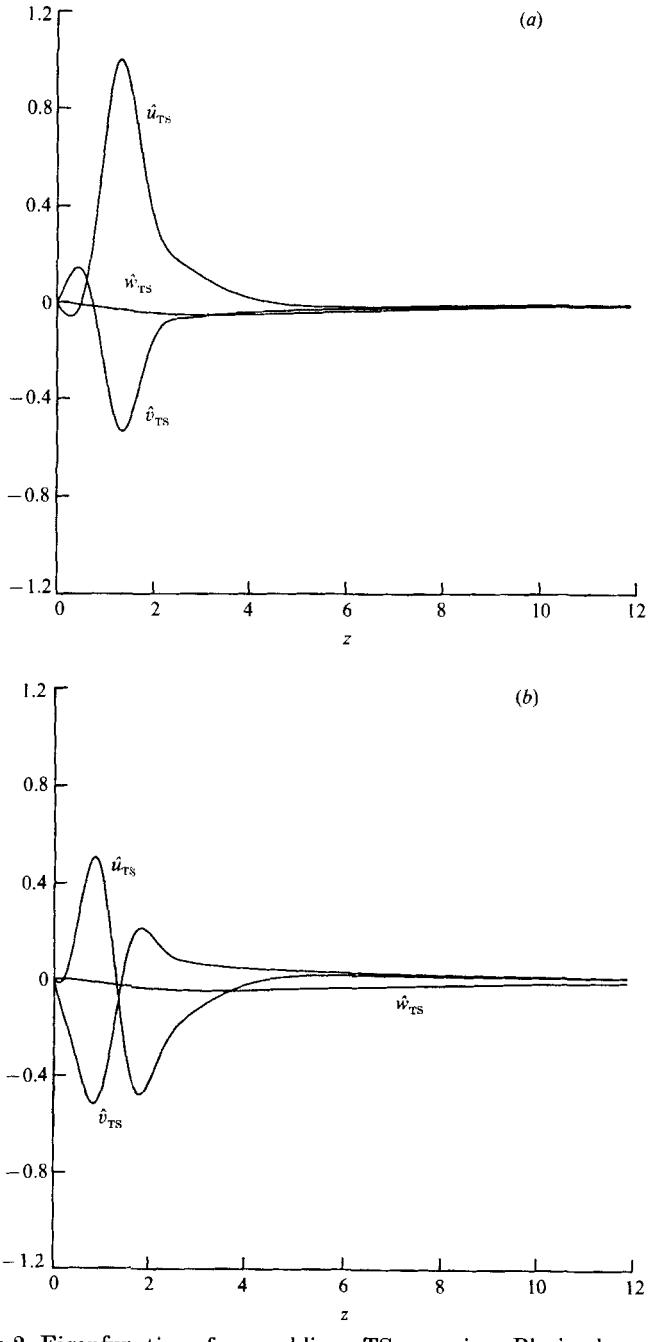

FIGURE 2. Eigenfunctions for an oblique TS wave in a Blasius boundary layer: $R = 950$, $\alpha = 0.103$, $\beta = 0.15$. (*a*) Real part, (*b*) imaginary part.

interaction of a Görtler vortex with two oblique TS waves may be studied by choosing the following initial conditions:

$$u(x,y,z,0) = U_B(z) + \epsilon_G \operatorname{Re}[\hat{u}_G(z)\,e^{i\beta_G y}] + \epsilon_{TS}\{\operatorname{Re}[\hat{u}(z)\,e^{i(\alpha_{TS}x+\beta_{TS}y)}] + \operatorname{Re}[\hat{u}(z)\,e^{i(\alpha_{TS}x-\beta_{TS}y)}]\}. \quad (2.17)$$

Various values of β_{TS} in relation to β_G may be assigned. For example, $\beta_{TS} = \frac{1}{2}\beta_G$ describes a subharmonic resonance and $\beta_{TS} = \beta_G$ describes a fundamental resonance. Relative magnitudes of ϵ_G and ϵ_{TS} describe various regimes of interaction where either the Görtler vortex or TS wave is small or when both have large amplitude and interact nonlinearly.

In the Navier–Stokes solution, the mean streamwise velocity U is allowed to develop in time according to

$$\frac{\partial U}{\partial t} = \frac{\partial^2 U}{\partial z^2} + F, \quad U(x, y, z, 0) = U_B(z). \tag{2.18}$$

Three different forms for the forcing term F were tried:

$$F = -\nu \frac{\partial^2 U_B}{\partial z^2} \tag{2.19}$$

$$F = 0, \tag{2.20}$$

$$F = -\nu \frac{\partial^2 U_B}{\partial z^2} + \frac{\partial U_B}{\partial t}, \tag{2.21a}$$

$$\frac{\partial U_B}{\partial t} = C_g \frac{\partial U_B}{\partial x}, \tag{2.21b}$$

where C_g is the disturbance group velocity defined above.

With (2.19), the mean velocity and the boundary-layer thickness does not change with time. The second condition ($F = 0$) alllows the boundary-layer thickness to increase and the long-time solution of (2.18) is given by the error function. Wray & Hussaini (1984) used this condition for their transition simulation in flat-plate boundary layers. The condition (2.21*a*) also allows the boundary-layer thickness to increase and is designed to give growth in time similar to the growth in space according to (2.21*b*). Since the solutions presented below are for short time only, all these formulations essentially gave the same results for the development of disturbances of different wavenumbers. Therefore, only the results obtained by using (2.19) are presented below.

Use of numerical simulation to study the intermodal interaction may be described best by providing the example of subharmonic instability in a flat-plate boundary layer. This instability, which is the result of parametric resonance between a two-dimensional TS wave and oblique TS waves with streamwise wavelength twice that of the fundamental wave, was first theoretically studied by Herbert (1984) using Floquet analysis. Here we consider the fundamental wave to have $\alpha = 0.2033$ and prescribe $R = 606$. An amplitude of 0.01 (i.e. 1%) is assigned to the two-dimensional TS wave.

According to Herbert, a strong subharmonic instability of wave numbers $(\frac{1}{2}\alpha, \beta)$ should develop for a wide range of β, (see figure 9 in Herbert 1984). The present calculation is performed by including in the initial conditions two oblique modes $(\frac{1}{2}\alpha, \beta = \pm 0.16968)$. Results of the calculation are presented in figure 3. In this figure, the natural logarithm of the energy history of the modes $(\alpha, 0)$ and $(\frac{1}{2}\alpha, \beta)$ are plotted as a function of time. Calculations are carried out to about 3.5 linear time periods of the finite-amplitude two-dimensional wave. The solid curves are the linear theory results for the corresponding modes. The finite-amplitude two-dimensional wave follows its linear growth ($\omega_i = 0.7 \times 10^{-5}$) curve within the computational domain.

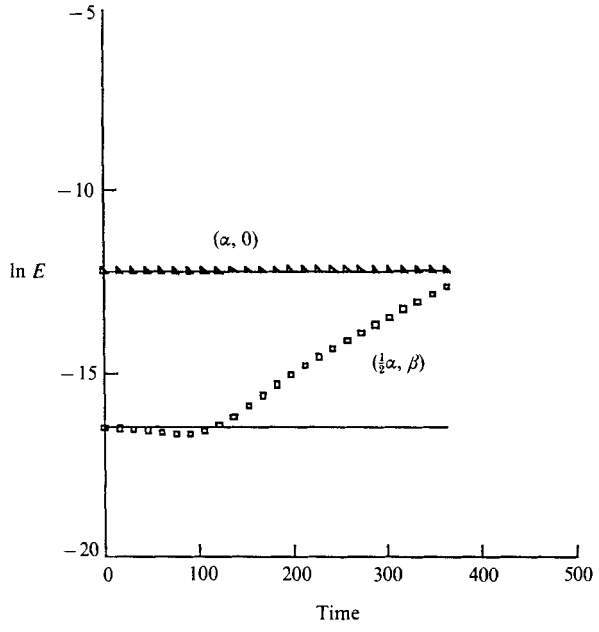

FIGURE 3. Computed evolution of energies of a two-dimensional TS wave ($(\alpha, 0)$ mode) and the oblique subharmonic ($(\frac{1}{2}\alpha, \beta)$ mode). In this calculation, $R = 606$, $\alpha = 0.2033$, $\beta = 0.16968$. A strong secondary subharmonic instability develops. Included in the initial conditions are two oblique primary subharmonics. The solid lines represent linear-theory results.

The subharmonic $(\frac{1}{2}\alpha, \beta)$ follows the linear theory result for the primary subharmonic for some time and then diverges from it indicating strong secondary instability. The growth rate at the onset of this instability is $\omega_i \approx 0.0098$ which drops to $\omega_i \approx 0.0071$ towards the end of the computation owing to nonlinear effects. This is in good agreement with the prediction of Herbert for $\omega_i = 0.00824$. The subharmonic secondary instability has been linked to the squire mode by Herbert (1984). However, in order to capture the instability using numerical simulations, we need not provide the actual eigenfunctions for the squire mode in the initial conditions. In our calculations we have used the eigenfunctions for the primary subharmonic. In another calculation the initial conditions for the $(\frac{1}{2}\alpha, \beta)$ modes were arbitrarily taken to be

$$\hat{u} = 0, \quad \hat{v} = z^2 \mathrm{e}^{-2(z-1)}, \quad \hat{w} = \pm \frac{\mathrm{i}}{\beta} \frac{\partial \hat{v}}{\partial y}. \tag{2.22}$$

The results are presented in figure 4. Again the subharmonic secondary instability emerges. Most interestingly, both calculations converge towards the same growth rate for the subharmonic. Higher harmonics also emerge in these nonlinear calculations. In a transition simulation, one would like to assign a small random distribution of energy to all the modes, except, of course, the finite-amplitude disturbance and let the dominant pattern evolve by itself. Such calculations for a flat-plate boundary layer have been done by Spalart (1985).

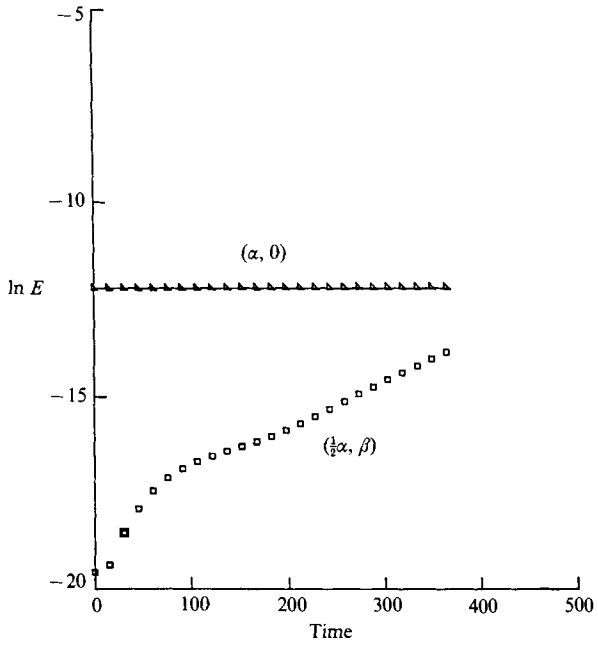

FIGURE 4. Same as for figure 3 except the initial conditions for the subharmonic were those given in (2.22).

3. Results for Görtler/TS interaction

3.1. *Subharmonic instability*

Using the multiple-scale method, Nayfeh (1981) and Srivastava & Dallmann (1987) presented results for Görtler/TS interaction in a boundary layer. Their results (derived from table 3 of Nayfeh 1981 and figure 5 of Srivastava & Dallmann 1987) for $R = 950$, $\beta = 0.3$ and $G = 14$ are given in figure 5 where the growth rate of the excited TS waves (in the presence of a Görtler vortex with 1% amplitude) of various frequencies is plotted. The growth rate of the excited TS waves are shown to increase dramatically in the presence of Görtler vortices. It was shown in Srivastava & Dallmann (1987) that the growth rate of the excited wave increases with decreasing Görtler number and increasing wavenumber β. The massive destabilization of the TS waves in the presence of Görtler vortices (with only 1% amplitude) shown in figure 5 is a bit surprising and of enormous concern to a designer. Here we choose this case ($R = 950$, $G = 14$, $\beta = 0.3$) for a direct numerical simulation.

The computed growth rate ω_i for the aforesaid case is 0.0033, which corresponds to a spatial growth rate of $\sigma = R\omega_i/C_g$ of 4.48 (C_g was computed for the Görtler vortex to be about 0.7). This is in reasonable agreement with the spatial calculations of Ragab & Nayfeh (1981). In the nonlinear simulations, the Görtler vortex is assigned an initial amplitude of 1%. The streamwise wavenumber α was taken to be 0.103. The complex frequency for the oblique $(\alpha, \frac{1}{2}\beta)$ mode is (0.038, 0.00079) and we assign to these oblique waves an initial amplitude of 0.1%. The calculation is performed by using eight Fourier modes in the streamwise direction, 16 modes in the spanwise direction and 33 Chebyshev polynomials across the boundary layer. Occasional tests of accuracy were made with twice the number of Fourier modes in the streamwise and spanwise directions and the growth rate results were essentially unaltered. In spectral methods, one can keep an explicit check on resolution by

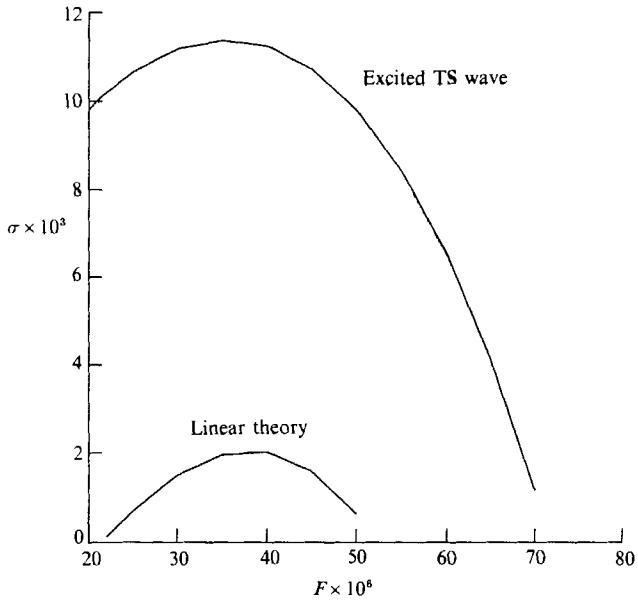

FIGURE 5. Spatial growth rates of excited oblique TS waves in the presence of a Görtler vortex with 1% amplitude (from Nayfeh 1981 and Srivastava & Dallmann 1987) and linear-theory results. As we show later, the curve labelled 'excited TS wave' is erroneous.

monitoring the energy content in the higher modes of the fourier–Chebyshev expansion. Furthermore, we also checked the results against linear stability theory and Herbert's secondary instability theory. The time evolution of the energy of six of the modes is presented in figure 6. The Görtler mode $(0, \beta)$ continues to grow according to its linear theory growth rate. No strong instability in the $(\alpha, \frac{1}{2}\beta)$ mode develops, at least within the computational period. The growth of this mode actually slows down slightly towards the end of the computational period. Similar growth behaviour of the $(\alpha, \frac{1}{2}\beta)$ mode was observed for other values of β at $\epsilon_G = 0.01$ and up to $\epsilon_G = 0.05$. The mode that grows the fastest is $(0, 2\beta)$, i.e. the one with half the wavelength of the finite-amplitude Görtler vortex. This seems to agree with the observation of Aihara & Koyama (1981) that the '... characteristic spanwise wavelength of importance is shown to be a half-wavelength of Görtler vortices in the present experiment'. Apparently, it is the nonlinear distortion of the Görtler vortex that is observed in Aihara & Koyama (1981). This nonlinear distortion of the finite-amplitude Görtler vortex is neglected in Nayfeh's theory. In our calculation, we also tried to 'simulate' Floquet theory by zeroing out all higher harmonics after each time step. Even this did not result in any change in the growth of the oblique TS waves. A careful look at the growth rates given in Nayfeh (1981) for the linear Görtler vortex and a comparison with Ragab & Nayfeh (1981) indicated that these growth rates could have been obtained only when the lengthscale $l = 1.72(\nu_\infty x/U_\infty)^{\frac{1}{2}}$ is used. The lengthscale used in Nayfeh (1981) for the TS problem was $l = (\nu_\infty x/U_\infty)^{\frac{1}{2}}$. It was noted by Malik (1986) that this discrepancy in the lengthscales may have been the cause for the erroneous growth rates computed by Nayfeh (1981). Indeed, this turned out to be the case. Nayfeh & Al-Maaitah (1987) later corrected the lengthscales and found that the multiple-scale analysis does not yield any excitation of the TS waves when the amplitude of the Görtler vortex is 1%. It is still not clear why the results of Srivastava & Dallmann (1987) agree with Nayfeh (1981).

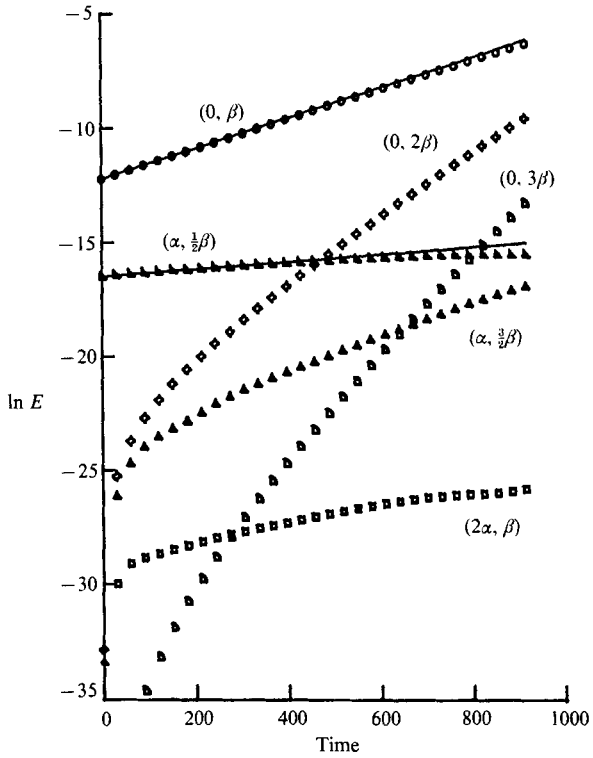

FIGURE 6. Computed evolution of energies of various modes in the presence of a Görtler vortex ((0, β) mode) with 1% amplitude in a two-dimensional boundary layer on a concave wall. Two oblique TS waves ((α, $\pm\frac{1}{2}\beta$) mode) with amplitudes of 0.1% are included in the initial conditions. In this calculation $R = 950$, $G = 14$, $\alpha = 0.103$, $\beta = 0.3$. The solid lines represent linear-theory results.

Srivastava & Dallmann also considered combination resonance and showed that it is a much more powerful instability mechanism than the subharmonic parametric resonance predicted by Nayfeh. They showed that the former mechanism produces growth rates which are an order-of-magnitude higher than the growth rates produced by the latter mechanism, given in figure 5. However, in view of the disagreement between their results and the present simulations of the subharmonic instability, the results of Srivastava & Dallmann for the combination resonance should be questioned. In any case, results presented by Nayfeh (1981) in tables 1–3 and by Srivastava & Dallmann (1987) in figures 1, 3 and 5 are erroneous.

The results for $\epsilon_G = 0.1$ for the above test case are presented in figure 7. Again, we note that the ($\alpha, \frac{1}{2}\beta$) mode does not grow faster than its linear theory results. So the resonance mechanism suggested by Nayfeh (1981) is not operative, at least at this wavenumber and amplitude of the Görtler vortex. Similar calculations using (α, $\pm\beta$) modes in the initial conditions did not indicate any resonant fundamental secondary instability. Later, we will show that the (α, β) mode is excited in the presence of a two-dimensional wave ((α,0) mode). Another calculation for the subharmonic instability is performed at this amplitude ($\epsilon_G = 0.1$) using $G = 12$ and $\beta_G = 0.15$. The streamwise wavenumber for the oblique TS wave is now $\alpha = 0.18$ and $R = 950$. The value of ω for this TS wave ($\alpha, \frac{1}{2}\beta$) is $\omega = (0.0628, -0.0002)$. So, this wave decays linearly. The results of the numerical simulation are presented in figure 8. Now the oblique TS wave is unstable, in qualitative agreement with the results of Nayfeh &

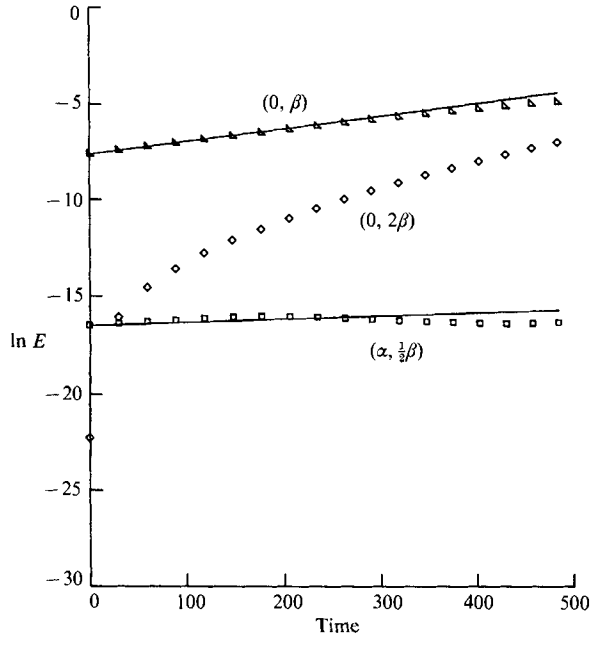

FIGURE 7. The effect of a Görtler vortex ($(0, \beta)$ mode) with 10% initial amplitude on oblique TS waves ($(\alpha, \frac{1}{2}\beta)$ mode). In this calculation, $R = 950$, $G = 14$, $\alpha = 0.103$, $\beta = 0.3$.

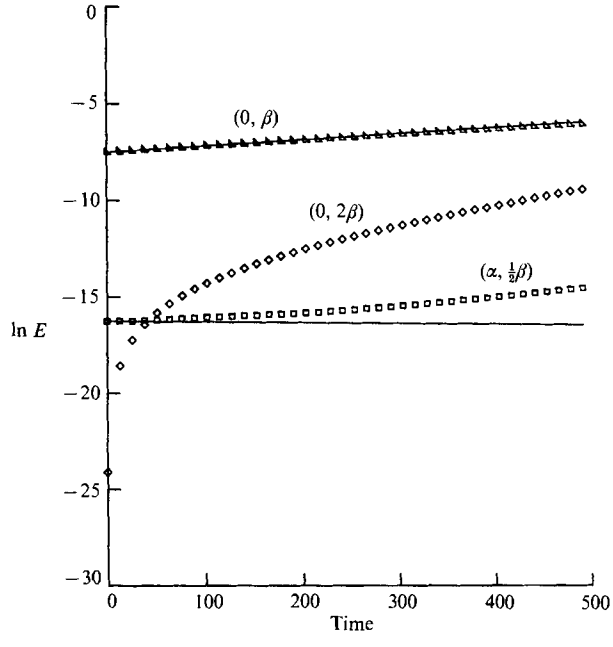

FIGURE 8. Same as figure 7 except that $G = 12$, $\alpha = 0.18$, $\beta = 0.15$.

Al-Maaitah (1987) using Floquet theory and multiple-scale analysis. However, the growth rates are no more than the growth rates of the primary Görtler instability. Apparently, the excitation of the subharmonic is more pronounced at smaller wavenumbers of the Görtler vortex for a given amplitude. This is also in direct

contradiction to the results of Srivastava & Dallmann who showed that the growth rates of the excited oblique wave increase with wavenumber. In any case, for some values of the parameters β and ϵ_G, the subhormonic resonance may be realized in the Görtler vortex breakdown. Evidently, the Görtler vortex amplitude needed for this to happen is in excess of 10%. This appears to be in qualitative agreement with the results of Nayfeh & Al-Maaitah (1988) who performed Floquet analysis to study the wave-interaction problem. Their results indicate that the excitation of TS waves is very weak at 1% amplitude of the Görtler vortex but it begins to become appreciable at high amplitudes of Görtler vortex. It may be noted that Nayfeh & Al-Maaitah only performed an analysis for $\beta = 0.154926$. Therefore, it is not known what trend their present Floquet theory would predict at higher wavenumbers β. As the Görtler vortex develops downstream, wavenumber β increases owing to the growth of the boundary layer and, since interaction takes place at relatively large amplitudes, the higher wavenumber regime would be more interesting. Since the normal mode approach for Görtler instability becomes questionable at low wavenumbers (Hall 1983) the results for only one value of β equal to 0.154926 does not have general validity. Since Nayfeh (1981) earlier had computed the $\beta = 0.3$ case and wrongly shown that the excitation of TS waves was more pronounced at this wavenumber, it is not clear to us why this wavenumber case was not repeated by Nayfeh & Al-Maaitah (1988).

3.2. *Other types of secondary instabilities*

Nonlinear development of Görtler vortices results in inflectional streamwise velocity profiles in the upwash region (peak plane) of the Görtler vortex flow. The inflection points caused by the presence of low-velocity fluid in the near-wall region of the peak planes appear both in the normal distribution $u(z)$ and the spanwise distribution $u(y)$ (see e.g. Swearingen & Blackwelder 1987). Localized inviscid secondary instabilities may be caused by these inflectional profiles. In the present instance, we use our numerical model to investigate possible excitation of two-dimensional $(\alpha, 0)$ disturbances in the flow field modulated by the presence of Görtler vortices. Calculation is first made for the same Görtler vortex as in the example of figure 8. The TS wave now has $\alpha = 0.18$ and the linear-theory eigenvalue $\omega = (0.0613, 0.0009)$. The results are presented in figure 9. The presence of the Görtler vortex causes the growth rate of the two-dimensional TS wave to increase above its linear theory value. The growth rate of the excited two-dimensional TS wave is comparable with the oblique subharmonic instability discussed above. Also shown in the figure are the computed growth history of the (α, β) mode. As noted before, this mode does not get excited in the absence of the $(\alpha, 0)$ mode. However, now the (α, β) mode attains higher growth rates in the presence of the $(\alpha, 0)$ mode. The growth rate of this mode is compared to other modes in figure 10 at time $t \approx 400$ (which is equivalent to about 4 periods of the two-dimensional mode) along with the corresponding linear-theory results. The figure also contains growth-rate results for the $(\alpha, \frac{1}{4}\beta)$ mode which is also excited.

Another calculation is performed at $G = 14$, $\beta_G = 0.5$ with the same amplitude for the Görtler vortex as before ($\epsilon_G = 0.1$). The two-dimensional TS wave now has $\alpha = 0.15$ and $\omega = (0.04940, 0.00227)$. The results are presented in figure 11. Again, the two-dimensional TS wave attains a growth rate much higher than its linear value. The (α, β) mode also grows fast owing to nonlinear interaction. The orientation $\psi = \tan^{-1}\beta/\alpha$ for this mode is 73.3°. The orientation of the (α, β) mode of figure 11 was 39.8°. So there seems to be a wide range of angles for which the (α, β) mode is unstable. In this example, the two-dimensional TS wave was linearly unstable.

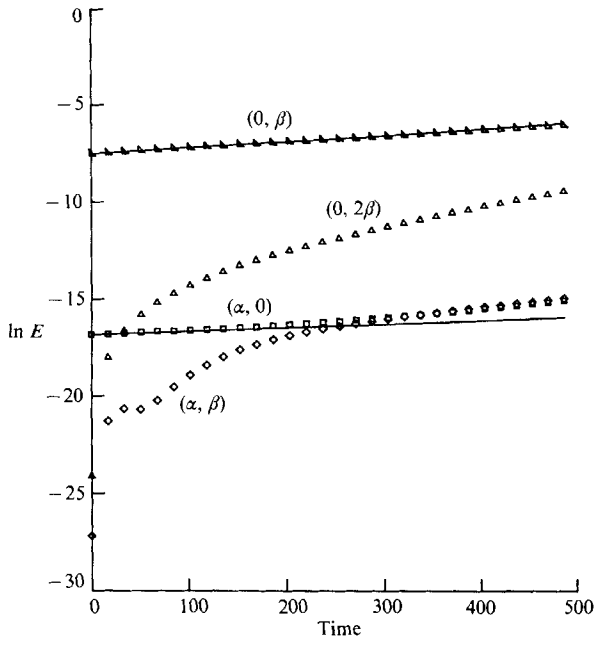

FIGURE 9. The effect of a Görtler vortex ($(0,\beta)$ mode) with 10% initial amplitude on a two-dimensional TS wave ($(\alpha,0)$ mode). In this calculation, $R = 950$, $G = 12$, $\alpha = 0.18$, $\beta = 0.15$. The (α,β) mode grows owing to nonlinear interaction. The solid lines represent linear-theory results.

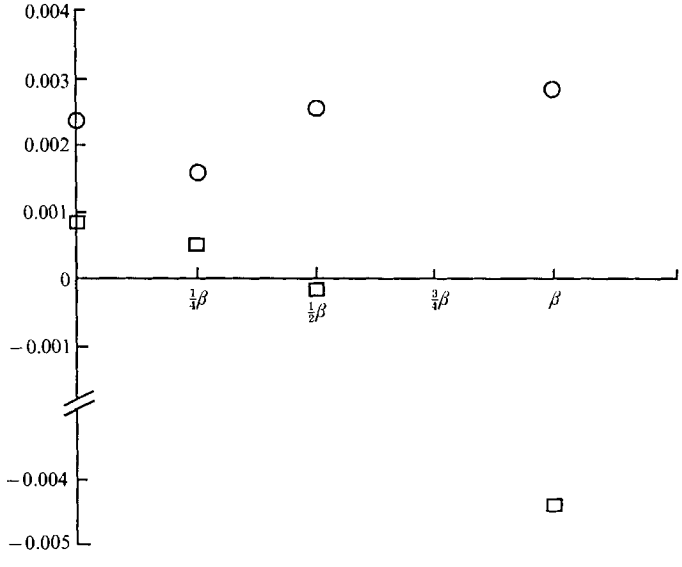

FIGURE 10. Temporal growth rates of various modes (with $\alpha = 0.18$) at time $t = 400$ in the presence of a Görtler vortex with $\beta = 0.15$. ○, Navier–Stokes; □, linear theory.

Another calculation is presented in figure 12 where the two-dimensional TS wave ($\alpha = 0.2$) is linearly stable (linear theory $\omega = (0.0693, -0.00115)$). As shown in the figure, both the $(\alpha,0)$ and (α,β) modes grow in the nonlinear calculations regardless of the fact that the TS mode chosen is linearly stable. This is consistent with the results presented in figures 3 and 4 where it was shown that the form of the initial

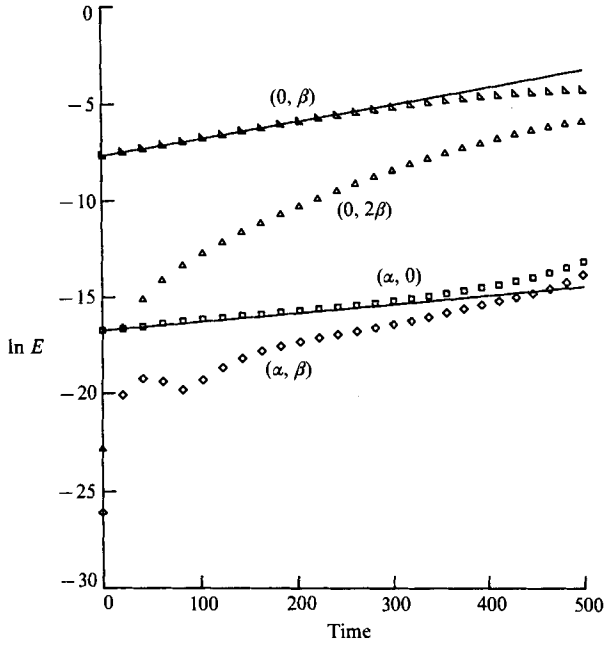

FIGURE 11. Same as figure 9 except that $G = 14$, $\alpha = 0.15$, $\beta = 0.5$.

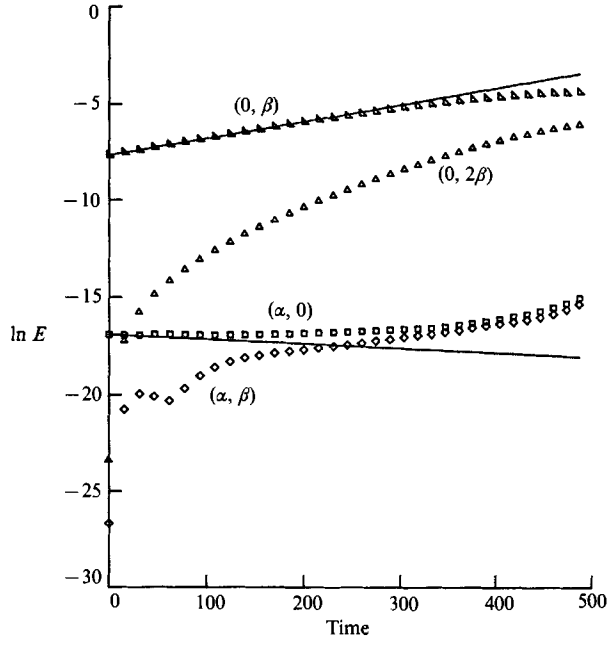

FIGURE 12. Same as figure 11 except that $\alpha = 0.2$.

conditions for the excited mode do not play a critical role. As noted previously, the first harmonic of the Görtler vortex gains energy faster than any other mode, indicating a spectral broadening process. However, the three-dimensionality and unsteadiness is caused by the development of $(\alpha, 0)$, (α, β) or possibly $(\alpha, \frac{1}{2}, \beta)$ modes, depending upon the initial conditions and flow parameters involved. The computed

growth rates of these excited modes, at least initially, remain small when compared to the growth rate of the Görtler vortex itself. However, the Görtler vortex does reach a saturated state (as also noted in the experiments of Swearingen & Blackwelder 1987) at which time the secondary instability modes will be expected to grow much faster and would lead to various kinds of breakdown mechanisms as observed by Swearingen & Blackwelder (1987), Bippes (1978) and Aihara & Koyama (1981). Calculations indicate that at saturation, the Görtler vortex amplitudes are in excess of 20%. We believe that our numerical model would be able to provide detailed qualitative information about the development of unsteadiness and eventual breakdown; however, this calculation would require much higher resolution than used here, especially in the normal direction, in order to resolve critical layers that are present near the edge of the boundary layer. With regard to the computational resources required, a calculation on a CRAY-2 computer would take about 1.2×10^{-4} seconds per node per time step.

4. Concluding remarks

Direct numerical simulation of wave interactions is useful not only in testing theories but also in bringing out new instability mechanisms in boundary layers. In this paper, we have presented a numerical model for Görtler/TS interaction which may be used to investigate various possible regimes of interactions between Görtler vortices and Tollmien–Schlichting waves. In the numerical examples, we have only considered the regime where Görtler vortices have finite amplitude and TS waves are relatively small. Even though our model is based upon the parallel-flow approximation, it provides the qualitative features of the possible interaction mechanisms. Of course, any mechanism that is mainly caused by non-parallel effects cannot be treated by our model. What mechanisms might be ruled out because of this limitation is open for discussion. Görtler/TS interaction takes place at relatively large amplitudes of Görtler vortices (as primary instability) and therefore secondary instability mechanisms leading to unsteadiness most likely involve nonlinearities, and the direct numerical simulation can obviously take account of such nonlinearities. Finally, we have found that the Görtler/TS interaction results presented by Nayfeh (1981) and Srivastava & Dallmann (1987) are erroneous. However, our calculations for subharmonic excitation are in qualitative agreement with the corrected results of Nayfeh & Al-Maaitah (1988).

This work was partly supported by NASA Contracts NAS1-18240 (MRM) and NAS1-18107 (MYH).

REFERENCES

Aihara, Y. & Koyama, H. 1981 *Trans. Japan Soc. Aero. Space Sci.* **24**, 78.

Bippes, H. 1978 *NASA TN*-75243.

Canuto, C., Hussaini, M. Y., Quarteroni, A. & Zang, T. A. 1988 *Spectral Methods in Fluid Dynamics*. Springer.

Floryan, J. M. & Saric, W. C. 1980 *AIAA Paper* 80-1376.

Hall, P. 1983 *J. Fluid Mech.* **130**, 41.

Hall, P. & Smith, F. T. 1988 *Proc. R. Soc. Lond.* A **417**, 244.

Herbert, T. 1984 *AIAA Paper* 84-0009.

Herbert, T. & Morkovin, M. V. 1979 *Laminar–Turbulent Transition* (ed. R. Eppler & H. Fasel), p. 37. Springer.

MALIK, M. R. 1986 *AIAA Paper* 86-1129.

MALIK, M. R., CHUANG, S. & HUSSAINI, M. Y. 1982 *Z. Angew. Math. Phys.* **33**, 189.

MALIK, M. R., ZANG, T. A. & HUSSAINI, M. Y. 1985 *J. Comput. Phys.* **61**, 64.

NAYFEH, A. H. 1981 *J. Fluid Mech.* **107**, 441.

NAYFEH, A. H. & AL-MAAITAH, A. 1987 *AIAA Paper* 87-1206.

NAYFEH, A. H. & AL-MAAITAH, A. 1988 *Phys. Fluids* **31**, 3543.

RAGAB, S. A. & NAYFEH, A. H. 1981 *Phys. Fluids* **24**, 1405.

SPALART, P. R. 1985 *9th Intl Conf. on Numer. Meth. in Fluid Dynamics* (ed. Soubbarameyer & J. P. Boujot), p. 531. Springer.

SRIVASTAVA, K. M. & DALLMANN, U. 1987 *Phys. Fluids* **30**, 1005.

SWEARINGEN, J. D. & BLACKWELDER, R. F. 1987 *J. Fluid Mech.* **182**, 255.

WRAY, A. & HUSSAINI, M. Y. 1984 *Proc. R. Soc. Lond.* A **392**, 373.

ZANG, T. A. & HUSSAINI, M. Y. 1985 *AIAA Paper* 85-0296.